THE INFLUENCE OF CONNECTED ELEMENTS ON THE FREQUENCY RESPONSE OF ROTATING MACHINES

Sandra Plötz[1*], Stephanie Uhrig[1]
[1]University of Applied Sciences Munich, Germany
[*]Email: ploetz.sandra@hm.edu

Avoiding unplanned downtime of rotating machines is becoming increasingly important as the demand for reliable operating processes grows. Various measurement methods are used in diagnostics, but most of these can only detect specific fault types. Frequency response analysis (FRA), is increasingly gaining attention in research on rotating machines, as it is able to identify a range of failure modes. Up until now, FRA has been used as an offline measurement method. The potential for implementing FRA in an online measurement setting is currently being explored. In both offline and online measurements, connected elements such as current and voltage transformers, supply lines with different properties, converters, sensors and mechanical components such as couplings or gearboxes can influence the measured frequency response. Since direct access to the terminal box without these external components is sometimes not possible in practice for both online and offline measurements, this work analyzes the impact of connected elements on the measured frequency response. The objective is to differentiate between damage to the machine and influence caused by the measurement setup or other electrically coupled components. For this purpose, measurements are carried out on machines with unshielded extensions of coaxial cables, antennas on the three-phase and field windings and various earthing configurations of the coaxial cables. The results are analyzed using an existing grey box model, which represents the characteristic features of the frequency response and could be extended to include the effects of antennas on the field winding. As a result, the influence of connected elements is shown both in measurement practice and in the theoretical model.

Keywords : FRA, ROTATING MACHINES, DIAGNOSTIC METHOD, CONNECTED ELEMENTS

1. Introduction

High-performance three-phase AC machines are essential for energy supply and industrial processes, and an unexpected failure can have considerable economic consequences. Early fault detection is therefore of great importance. Previous studies have shown that frequency response analysis (FRA) is a promising method for diagnosing the condition of rotating machines [1], [2], [3], [4]. While FRA is already standardized and established for power transformers [5], [6], there are no comparable standards for its application on rotating machines. Standardizing SFRA measurements on rotating machines could reduce application errors and improve comparability. Clear guidelines on measurement setup, wiring and documentation would avoid inconsistent measurement settings and increase the reliability of measurement results.

The evaluation of the FRA is based on the comparison of a recent measurement with a reference measurement. Deviations between two frequency response traces indicate changes in the electrical network that can have mechanical, electrical or electromagnetic causes. These changes allow conclusions to be drawn about potential damage and its possible cause. As this is a comparative method, the choice of a suitable reference measurement is crucial, as even minor deviations can lead to a change in the frequency response.

Measuring the frequency response currently requires the machine to be disconnected from the power supply and connected components to be disconnected, which involves considerable effort. An online monitoring system is desirable to achieve seamless monitoring. The extent to which the FRA method is suitable for online use is therefore currently being investigated [7]. However, in both offline and online measurements, connected elements such as current and voltage transformers, supply lines or mechanical components such as couplings or gearboxes influence the frequency response. It is therefore essential to clearly distinguish effects from the measurement setup or electrically coupled components from actual machine damage.

This paper investigates the influence of connected elements on the frequency response, with a focus on the wiring.

2. Basics of the SFRA method

For sweep frequency response analysis (SFRA), a sinusoidal voltage of, for example, 10 V_{PP} with a known phase shift is applied on the input terminal of a three-phase winding (U_1) and is measured on the output terminal (U_2) after passing through the three-phase winding. The input signal sweeps through a predefined frequency range from 20 Hz to 2 MHz. Depending on the frequency, the input signal is attenuated in amplitude and shifted in phase (Fig. 1). The resulting attenuation D(f) ([D] = dB) and the phase shift φ(f) ([φ] = deg) can be determined and evaluated.

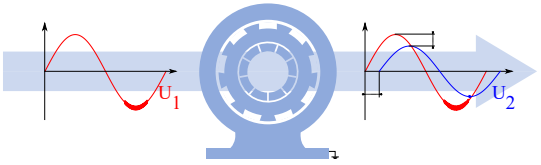

Fig. 1. Schematic illustration of the SFRA measuring method [8].

A frequency response is evaluated by a time-, phase- or type-based comparison or by comparing several measurements with

different defined rotor positions.

Each machine has an individual frequency response, which is not identical even for sister machines. However, previous studies have shown that, regardless of the power class, machine size or design, four characteristic frequency ranges occur for synchronous machines and three for induction machines (Fig. 2): the low-pass behavior (red, first range), the double resonance (green, second range, not present for induction machines), the local maximum (yellow, third range) and the main resonance (blue, fourth range) [4], [9]. The characteristics and precise frequency ranges differ for each machine, but they are similar for identically constructed machines.

The low-pass behavior is caused by the inductance on the stator side and the copper resistance. The double resonance is induced by a resonance on the rotor side, which is transferred to the stator side by the inductances on the rotor and stator sides. There is no double resonance if synchronous machines with short-circuited field windings or induction machines with squirrel-cage rotors are examined. The local maximum is strongly influenced by the earthing of the machine housing. The main resonance is the most pronounced resonance point of the stator winding. [4], [10]

Some characteristic ranges show a dependency on the rotor angle, i.e. the damping within a frequency range varies depending on the relative position of the rotor to the stator. For certain types of faults, such as a broken bar in the damper cage of a synchronous machine, it is necessary to carry out measurements over the entire rotor angle. [3], [8], [11]

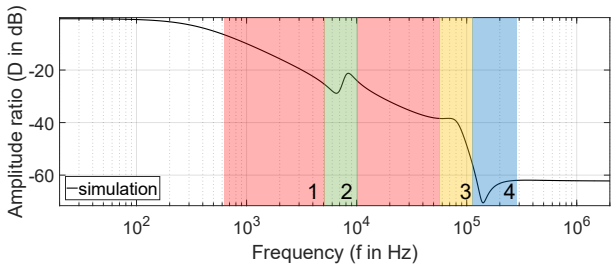

Fig. 2. General behavior of the FRA trace of rotating machines.

In order to be able to attribute deviations between two measurements to specific faults, the characteristic ranges of the frequency response are simulated. This provides a better understanding of the response shape, as it can be traced back to the components of an RLC network. The simulation can also help to simplify the evaluation of the measurements or to standardize them in the long term. A single-phase grey box model is used for this purpose, which maps the characteristic ranges of the frequency response and thus simulates the general trace (Fig. 3). The index "S" describes stator-side parameters, the index "F" rotor-side parameters. The area marked in red represents the measurement setup and is not part of the machine model. The meaning of the model parameters is described in Table 1.

The single-phase grey box model used is intended to simulate the essential characteristics of synchronous and induction machines of different power classes, sizes and designs. Due to the simplification of the model, it is not possible to reproduce the measurements exactly in all ranges. A more precise reproduction would require an individually adapted white box model, which would involve significantly more effort. The choice of model type therefore represents a compromise between complexity and accuracy. Deviations are to be expected, particularly at high frequencies above the main resonance, as this range would require a very high effort for exact modelling [12].

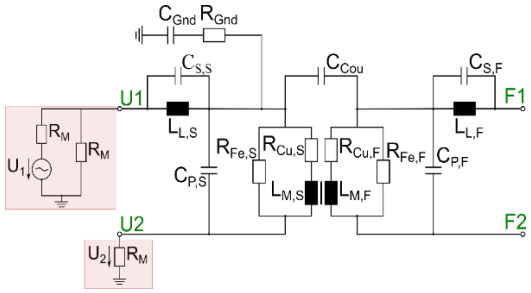

Fig. 3. Single-phase grey box model [8].

Table 1. Model parameters of the single-phase grey box model.

Component	Meaning of the components
L_L, C_S	Leakage inductance of the considered winding with corresponding series capacitance
R_{Gnd}, C_{Gnd}	Stator winding to ground coupling
R_{Fe}	Represent the iron losses due to magnetic flux
R_{Cu}, L_M	Copper resistance and main inductance
C_P	Parallel capacitance
C_{Cou}	Capacitive coupling between stator and rotor

3. Influence of connected elements

To illustrate the modifications to the individual parameters, the respective setup is shown in a figure, with adjustments marked in green. Fig. 4 shows the basic setup without variations. The measuring device is shown on the left and an electrically excited synchronous machine on the right. The star-point of the stator is not connected and all windings operate in an open-circuit. The measurement setup, particularly the measurement device in Fig. 4, is taken into account by the red boxes in Fig. 3.

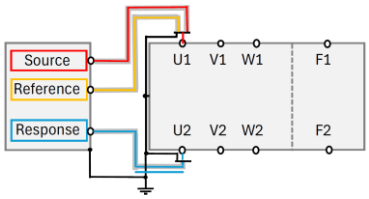

Fig. 4. Schematic illustration of the measurement setup without configurations.

The measurements are performed using the Franeo 800 from OMICRON electronics GmbH. It has three ports: Source, Reference and Response. The input signal is applied to the input terminal e.g. U_1 via Source, while the output signal is measured at e.g. U_2 via Response. The reference signal is also applied to U_1 and is used to minimize errors by counter-measuring the input signal. Source and reference are connected via a BNC T-piece and are connected to the corresponding terminal of the terminal box using an alligator clip. For the signal wires, shielded coaxial cables with BNC connectors (L = 5 m; Z_0 = 50 Ω) are used. The shield of the coaxial cable (gray outline in Fig. 4) is tapped at the BNC T-piece and connected to the grounding of the machine and measuring device (black lines).

All measurements performed are single-phase measurements with an open field winding. Only the attenuation is shown in the figures, as the phase shift can be extracted from the attenuation and does not provide any additional information in this context [13].

3.1 Test objects The investigations for different cable configurations were carried out on a synchronous machine (SM) with 25 kVA (SM 1), while the connected measuring devices were examined on SM 2 (3.8 MVA). An overview of the most important technical data can be found in Table 2.

Table 2. Overview of the nominal data of the machines under investigation.

	Voltage	Power	Speed	cos(φ)
SM 1	(Y) 380 V	25 kVA	1500 rpm	1
SM 2	(III) 953 V	3.8 MVA	1500 rpm	0.997

3.2 Influence of connected cables A total of six different measurement setups are examined. The initial focus is on coaxial cables with partially unshielded wires to simulate practical setup challenges, followed by an analysis of the influence of antennas on the machine and the grounding of the coaxial cables. The term "antennas" here refers to cables that are connected to the terminals of the machine but remain open or unconnected at the end. Such antennas are created when cables are disconnected from sensors, inverters or similar devices.

a) Unshielded extension of coaxial cables: The unshielded extension of the coaxial cable is inserted behind the BNC T-piece (Fig. 5, green cable). The unshielded cable at U_1 always has the same length as the cable at U_2. Extensions from 50 cm to 30 m with a cable cross-section of 2.5 mm² are considered.

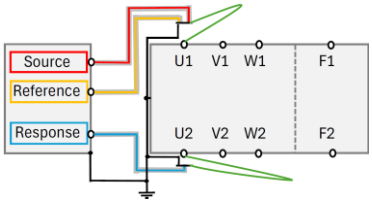

Fig. 5. Schematic illustration of the measurement setup with partially unshielded signal cables.

The black curve always represents the reference, which was recorded without the influence of additionally connected elements. Fig. 6 shows the measurements with unshielded cables in lengths from 2 m to 30 m. The designation "SRR" stands for the extension of the signal wires of the input (source & reference) and output (response) signals.

For unshielded cables up to a length of 6 m, a clear shift in the measurement can be seen above 600 kHz. The shape of the curve remains largely constant, while the attenuation decreases. Even at lower frequencies at the local maximum (230 kHz) and the main resonance (490 kHz), minimal deviations are recognizable. With an extension to 30 m, the frequency response changes at significantly lower frequencies (from 105 kHz), with attenuation deviations of up to 4 dB and the curve shows significant deviations: The local maximum shifts to lower frequencies and attenuations, the main resonance is attenuated less, and the behavior after the main resonance shows a changed shape at lower attenuations.

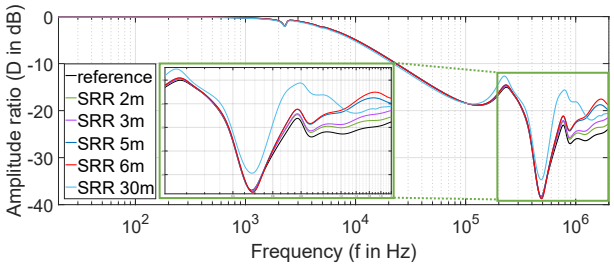

Fig. 6. Influence of partially unshielded signal cables.

b) Antennas: Fig. 7 illustrates the schematic measurement setup for antennas connected to the terminals of the three-phase windings. The antennas are connected exclusively to the inputs of all three-phase windings (U_1, V_1, W_1) and were extended in equal steps of 4 m.

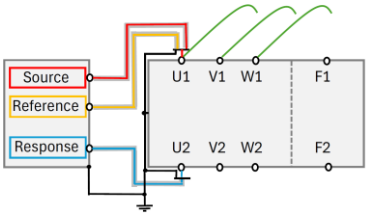

Fig. 7. Schematic illustration of the measurement setup with antennas connected to the three-phase windings.

Fig. 8 shows that the antennas already cause small deviations from the reference measurement at frequencies starting at 100 kHz. The deviations increase with increasing frequency.

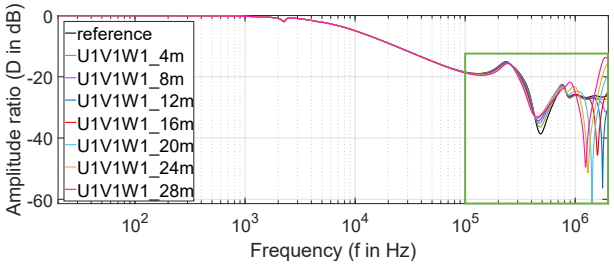

Fig. 8. Influence of antennas connected to the three-phase windings.

The arrows in Fig. 9 (close-up of Fig. 8) illustrate the changes in the frequency responses as a proportion of the length of the antennas. Particularly noticeable is the additional resonance that develops in the frequency range between 1.25 MHz and 1.77 MHz.

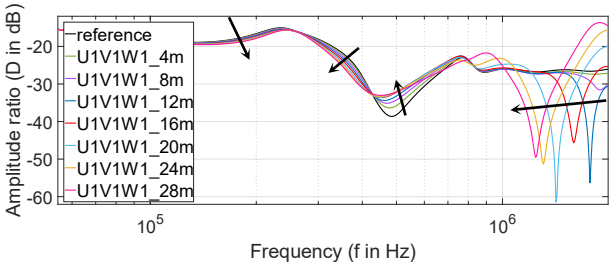

Fig. 9. Close-up of the area outlined in green in Fig. 8 with arrows showing the changes with increasing antenna length.

In a further measurement campaign, antennas were installed on the field windings and extended in 4 m steps (Fig. 10).

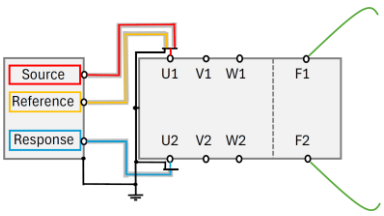

Fig. 10. Schematic illustration of the measurement setup with antennas connected to the field winding.

Fig. 11 shows that antennas on the field winding shift the double resonance (1.6 kHz - 2.7 kHz) towards lower frequencies with increasing length and exhibit lower attenuation. Although the antenna was extended in equal 4 m steps, the shift of the double resonance is not linear; at the beginning the shift is stronger (Δ 69 Hz) and decreases with increasing length (Δ 46 Hz). In addition, a weakly pronounced resonance at 4.9 kHz shifts to lower attenuations with increasing cable length. All other frequency ranges show no changes.

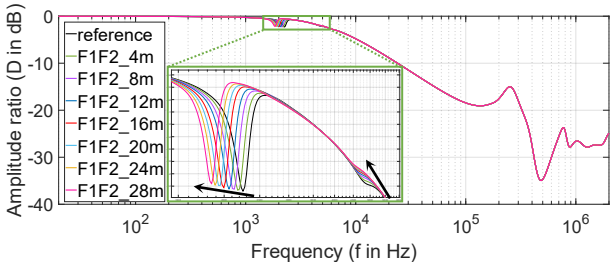

Fig. 11. Influence of antennas connected to the field winding.

c) Earthing of the coaxial cable: As electrical grounding was not explicitly shown in the previous figures, the illustration has been adapted to show the earthing of the coaxial cables (Fig. 12). Fig. 12 a) shows the representation used in the previous figures, while the implementation on Fig. 12 b) corresponds to the representation for the investigation of the earthing of the coaxial cables. The signal lines remain unchanged.

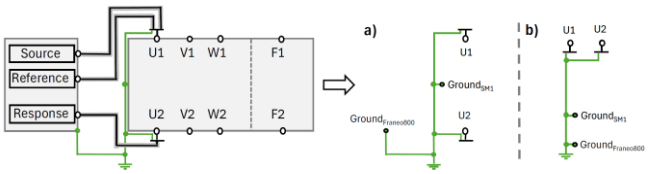

Fig. 12. Adapted illustration of the earthing concept.

In the first configuration, the shields of the coaxial cables are connected at one point and then routed together to the grounding of the machine and the measuring device (Fig. 13 a)). Here, the cable length L_1 remains constant (L_1 = 0.25 m; R_{L1} = 6 mΩ), while L_2 is varied in length.

In the second configuration, the shields of the coaxial cables are routed separately to the grounding of the machine and the measuring device (Fig. 13 b)). The cable lengths of the earthing conductors are the same for a measurement and their lengths are varied collectively for the next measurements ($L_{2\_U1} = L_{2\_U2}$). It is also investigated whether there is a difference depending on the distance between the two cables (1st case: L_1 < 5 cm; 2nd case: L_1 > 5 cm).

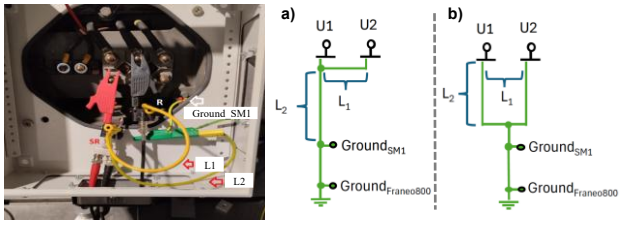

Fig. 13. Illustration of the measurement setup with configurations of the earthing path.

Fig. 14 shows that changing the earthing according to the schematic in Fig. 13 a) affects the attenuation from a frequency of 1 MHz by increasing it. With a cable length of 1.5 m or more, however, the attenuation decreases again at 1.9 MHz. In all other frequency ranges, no changes can be observed.

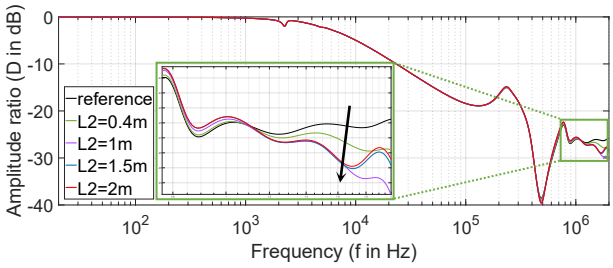

Fig. 14. Influence of the adapted earthing according to Fig. 13 a) with L_1 = const.

Fig. 15 shows the frequency responses according to Fig. 13 b) with different curves above 1 MHz, which depend on the distance and length of the earthing cables. The red/orange curves represent a cable distance of more than 5 cm, while the blue/green curves stand for less than 5 cm. The length of L_2 was also varied. The frequency responses with a smaller distance (L_1 < 5 cm) have a higher attenuation than the measurements with a distance of more than 5 cm. If L_2 is increased, the attenuation increases above 1 MHz for all measurements. All other frequency ranges show no changes.

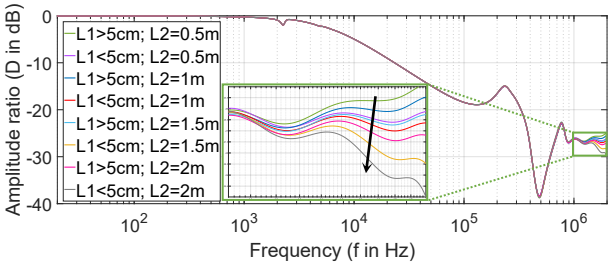

Fig. 15. Influence of the adapted earthing according to Fig. 13 b) with L_1 < 5 cm and L_1 > 5 cm.

3.3 Influence of additional measurement devices

The measurements in this chapter were performed to identify a possible rod fracture in the damper cage of SM 2. As described in chapter 2, such an analysis requires measurements over the entire rotation angle [3], [8], [14]. A suitable procedure is to carry out the measurements in 10° steps, so that a total of 36 measurements are required for a complete recording of the three-phase winding over 360°.

In order to reduce the time and organizational effort involved in these measurements on a 3.8 MVA machine, an optimized measurement setup was tested in 2024. Instead of working with just one Franeo 800, three Franeo 800 from OMICRON electronics

GmbH were used parallel (Fig. 16). The three-phase windings that were not measured were each connected to an inactive Franeo 800. This procedure made it possible to examine the other windings directly after measuring one winding without changing the rotor position. This meant that only a single rotor turning was required to perform 108 measurements, which significantly reduced the measurement effort.

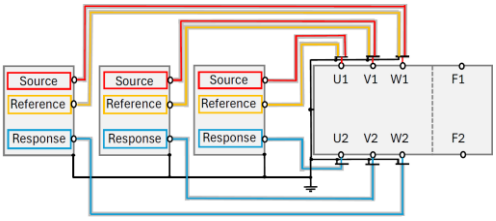

Fig. 16. Schematic illustration of the measurement setup with three connected measuring devices.

The evaluation resulted in the measurements from 2024 (2024_1) showing significant deviations from the reference measurements from 2021 (Fig. 17). These differences occurred in all characteristic ranges but were particularly pronounced in the frequency range between 4 kHz and 300 kHz.

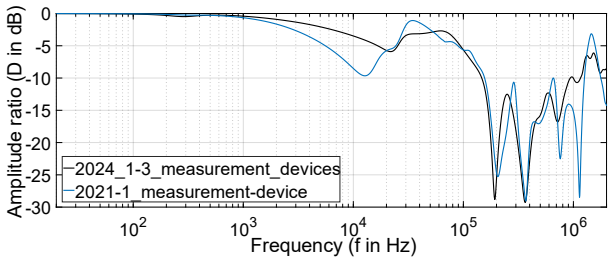

Fig. 17. Influence of three connected measuring devices.

The effect was confirmed by renewed measurements at a later date (2024_2) (Fig. 18). Both, the original reference measurement from 2021 (with one Franeo 800) and the optimized measurement from 2024 (with three parallel Franeo 800), could be reproduced. In both cases, similarly strong deviations occurred over the entire frequency range, particularly clearly between 700 Hz and 300 kHz.

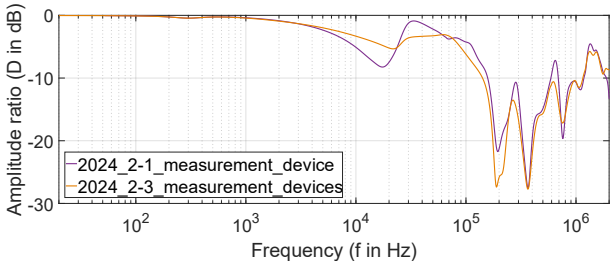

Fig. 18. Reproduced measurements with connected measuring devices.

4. Discussion

4.1 Analysis and comparison of the results with the simulation model The influences of unshielded extensions of coaxial cables, antennas connected to the three-phase windings and the earthing of the coaxial cables are particularly present at high frequencies after the main resonance, as this is where the inductances have their largest influence. As described in chapter 2, the model is limited in this range and cannot exactly reproduce the effects after the main resonance. In contrast, the effects of antennas on the field winding already occur at significantly lower frequencies at the double resonance. As most of the faults investigated occur in lower frequency ranges [14], the fault diagnostics remain largely unaffected by the stator-side configurations.

Shifting only the double resonance corresponds to the understanding of the model, as only this range is suitable for representing rotor-side effects in the model. The simulation for modelling the antenna on the field winding is shown in Fig. 19, based on the model parameterization according to [10]. The observed shift of the double resonance can be simulated by adding a capacitor (C1) to the model, which represents the capacitance between the antennas. In the simulation, the capacitance gradually increased by 122 pF to simulate the effect of the measurement.

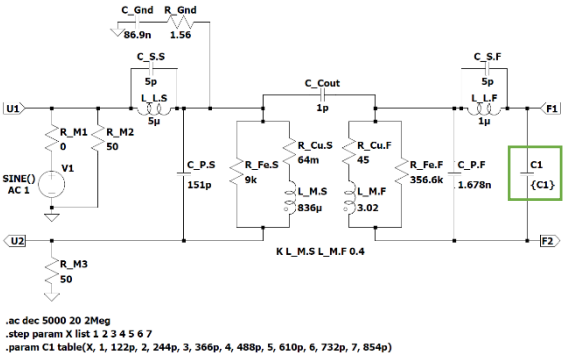

Fig. 19. Simulation of the single-phase grey box model with addition of capacitor C1 to simulate antennas on the field winding.

Fig. 20 shows that the shift of the double resonance can be reproduced by this extension of the model. The additional smaller double resonance that occurs in the measurement is not taken into account in the modeling.

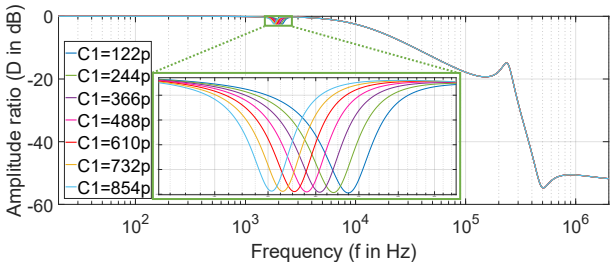

Fig. 20. Simulation results for replicating antennas on the field winding.

It is not yet possible to simulate the measurements with three measuring devices, as the measuring devices form a complex electrical network. Further detailed investigations are necessary to simulate this configuration adequately.

4.2 Recommendations for the performance of measurements A consistent and well-documented measurement setup is essential for reliable and reproducible measurement results in SFRA. Influencing factors, especially at high frequencies, are often difficult to clearly assign, as different causes can produce similar effects. In order to be able to interpret measurement deviations correctly, all relevant influencing factors should therefore be described in detail and ideally documented with images. Passive measuring devices, which are connected to open windings during single-phase measurement, can significantly

change the frequency response. An identical measurement setup with regard to measuring devices and cabling is therefore essential. If a measurement is carried out under inconsistent or undocumented conditions, it cannot be used for condition diagnostics.

As changes in the earthing path can influence the frequency response at high frequencies, the earthing should always be laid as identically as possible. It is recommended to always choose the shortest path for earthing in order to minimize unwanted effects and to ensure uniform cable routing.

4.3 Outlook For antennas on the three-phase windings, additional resonances occurred above 1 MHz, the origin of which is currently unclear. It is possible that these resonances already existed without antennas at higher frequencies above the measurement range or were caused by an additional resonant circuit. A more precise analysis of this effect requires measurements in an extended frequency range.

As only two synchronous machines were examined as test objects, further measurements are required to confirm that the cabling changes also have similar effects on other machines. However, due to the similarity of the machine characteristics [15] comparable effects on the frequency response are assumed.

Further investigations into connected elements and influencing factors are intended, as different inverters or sensors can influence machines in different ways. In addition, the identified influences should be verified with other measurement configurations, such as star measurements instead of single-phase measurements, to check whether the same effects occur.

5. Summary

The SFRA is evaluated by comparing a measurement with a reference measurement, with deviations indicating potential faults in the machine. It is therefore essential to distinguish between measurement-related influences and actual damage. In this work, the effects of additionally connected cables and measuring devices are investigated. Unshielded extensions of coaxial cables, antennas on the three-phase and field windings and different earthing configurations of the coaxial cables were observed.

The investigations showed that changes on the stator side - including unshielded signal wires, antennas on the three-phase windings and different earthing configurations - lead to a change in attenuation after the main resonance. Antennas on the field winding, on the other hand, cause a shift in the double resonance, an effect that could be reproduced by simulations. The influence of additional measuring devices extends over almost the entire frequency range and can lead to significant deviations.

A measurement setup that is as consistent as possible is crucial for reliable SFRA measurements. All potential influencing factors should be kept constant and comprehensively documented to enable a clear distinction to be made between actual machine damage and measurement-related effects.

6. Acknowledgments

This publication was developed as part of the EFRoM research project, funded by the German Federal Ministry of Education and Research. The authors would also like to thank those who provided test objects and equipment for measurements: OMICRON electronics GmbH and voestalpine AG.

References

[1] S. Uhrig, F. Ottl, R. Hinterholzer, and N. Augeneder, “Reliable Diagnostics on Rotating Machines using FRA,” in 2020 International Conference on Diagnostics in Electrical Engineering (Diagnostika), Pilsen, Czech Republic: IEEE, Sep. 2020, pp. 1–6. doi: 10.1109/Diagnostika49114.2020.9214647.

[2] F. Ciancetta, A. Del Pizzo, C. Olivieri, N. Rotondale, L. Castellini, and M. d’Andrea, “SFRA technique applied to fault diagnosis on stators of electric motors,” in 2014 International Symposium on Power Electronics, Electrical Drives, Automation and Motion, Ischia, Italy: IEEE, Jun. 2014, pp. 515–520. doi: 10.1109/SPEEDAM.2014.6871937.

[3] C. A. Platero, F. Blázquez, P. Frías, and D. Ramírez, “Influence of Rotor Position in FRA Response for Detection of Insulation Failures in Salient-Pole Synchronous Machines,” IEEE Trans. Energy Convers., vol. 26, no. 2, Art. no. 2, Jun. 2011, doi: 10.1109/TEC.2011.2106214.

[4] L. Ranzinger, I. Stephanie Uhrig, and F. Öttl, “Basic behaviour of FRA measurements on rotating machines,” in 22nd International Symposium on High Voltage Engineering (ISH 2021), Hybrid Conference, Xi’an, China: Institution of Engineering and Technology, 2021, pp. 24–29. doi: 10.1049/icp.2022.0004.

[5] T. M. Rao, S. Mitra, and S. Pramanik, “An Improved Method for Identification of Mechanical Damage in an Isolated Transformer Winding Using FRA,” in 2022 IEEE 6th International Conference on Condition Assessment Techniques in Electrical Systems (CATCON), Durgapur, India: IEEE, Dec. 2022, pp. 268–272. doi: 10.1109/CATCON56237.2022.10077689.

[6] P. Picher, C. Rajotte, and C. Tardif, “Experience with frequency response analysis (FRA) for the mechanical condition assessment of transformer windings,” in 2013 IEEE Electrical Insulation Conference (EIC), Ottawa, ON, Canada: IEEE, Jun. 2013, pp. 220–224. doi: 10.1109/EIC.2013.6554237.

[7] G. Bucci, F. Ciancetta, and E. Fiorucci, “Apparatus for Online Continuous Diagnosis of Induction Motors Based on the SFRA Technique,” IEEE Trans. Instrum. Meas., vol. 69, no. 7, pp. 4134–4144, Jul. 2020, doi: 10.1109/TIM.2019.2942172.

[8] L. Ranzinger, S. Uhrig, S. Tenbohlen, and F. Öttl, “Einfluss des Rotordrehwinkels auf die Frequenzantwort von Synchronmaschinen,” Berlin, Germany, 2022.

[9] S. Plötz, L. Ranzinger, and S. Uhrig, “Frequency Response Analysis on Rotating Machines – Model Parameterization for Different Machine Types and Performance Classes,” in 2024 International Conference on Diagnostics in Electrical Engineering (Diagnostika), Pilsen, Czech Republic: IEEE, Sep. 2024, pp. 01–06. doi: 10.1109/Diagnostika61830.2024.10693894.

[10] S. Plötz, L. Ranzinger, and S. Uhrig, “Frequency response analysis on rotating machines – model parameterization for different machine types and performance classes,” München, Germany, 2024.

[11] L. Ranzinger, S. Uhrig, R. Hinterholzer, and F. Öttl, “Failure diagnosis in rotating machines using fra involving the rotation angle of the rotor,” in 22nd International Symposium on High Voltage Engineering (ISH 2021), Hybrid Conference, Xi’an, China: Institution of Engineering and Technology, 2021, pp. 486–491. doi: 10.1049/icp.2022.0049.

[12] M. Heindl, S. Tenbohlen, and R. Wimmer, “Transformer modeling based on standard frequency response measurements,” Hannover, Germany, 2011.

[13] G. Lehner, Elektromagnetische Feldtheorie, 9. Auflage. Berlin: Springer Vieweg, 2021.

[14] L. Ranzinger, S. Uhrig, and S. Tenbohlen, “Analysis and Modeling the Frequency Response of Rotating Machines Regarding Fault Diagnosis Using SFRA,” in IEEE Transactions on Energy Conversion, Mar. 2024, pp. 747–756. doi: 10.1109/TEC.2023.3315341.

[15] L. Ranzinger, S. Uhrig, S. Tenbohlen, and S. Plötz, “Transferability of SFRA Measurements Between Rotating Machines of Different Power Class and Type,” in 2024 International Conference on Diagnostics in Electrical Engineering (Diagnostika), Sep. 2024, pp. 1–6. doi: 10.1109/Diagnostika61830.2024.10693884.